IL-4/STAT6 signaling facilitates innate hematoma resolution and neurological recovery after hemorrhagic stroke in mice

Jing Xu[a,1], Zhouqing Chen[a,1], Fang Yu[a,1], Huan Liu[a], Cheng Ma[a], Di Xie[a], Xiaoming Hu[a,b], Rehana K. Leak[c], Sherry H. Y. Chou[a], R. Anne Stetler[a,b], Yejie Shi[a,b], Jun Chen[a,b], Michael V. L. Bennett[d,2], and Gang Chen[a,2]

[a]Department of Neurology, Pittsburgh Institute of Brain Disorders & Recovery, University of Pittsburgh, Pittsburgh, PA 15213; [b]Geriatric Research, Education and Clinical Center, Veterans Affairs Pittsburgh Health Care System, Pittsburgh, PA 15261; [c]Graduate School of Pharmaceutical Sciences, School of Pharmacy, Duquesne University, Pittsburgh, PA 15282; and [d]Dominick P. Purpura Department of Neuroscience, Albert Einstein College of Medicine, Bronx, NY 10461

Contributed by Michael V. L. Bennett, November 1, 2020 (sent for review September 2, 2020; reviewed by Cesar Borlongan and Hua Su)

Intracerebral hemorrhage (ICH) is a devastating form of stroke affecting millions of people worldwide. Parenchymal hematoma triggers a series of reactions leading to primary and secondary brain injuries and permanent neurological deficits. Microglia and macrophages carry out hematoma clearance, thereby facilitating functional recovery after ICH. Here, we elucidate a pivotal role for the interleukin (IL)-4)/signal transducer and activator of transcription 6 (STAT6) axis in promoting long-term recovery in both blood- and collagenase-injection mouse models of ICH, through modulation of microglia/macrophage functions. In both ICH models, STAT6 was activated in microglia/macrophages (i.e., enhanced expression of phospho-STAT6 in Iba1$^+$ cells). Intranasal delivery of IL-4 nanoparticles after ICH hastened STAT6 activation and facilitated hematoma resolution. IL-4 treatment improved long-term functional recovery in young and aged male and young female mice. In contrast, STAT6 knockout (KO) mice exhibited worse outcomes than WT mice in both ICH models and were less responsive to IL-4 treatment. The construction of bone marrow chimera mice demonstrated that STAT6 KO in either the CNS or periphery exacerbated ICH outcomes. STAT6 KO impaired the capacity of phagocytes to engulf red blood cells in the ICH brain and in primary cultures. Transcriptional analyses identified lower level of IL-1 receptor-like 1 (ST2) expression in microglia/macrophages of STAT6 KO mice after ICH. ST2 KO diminished the beneficial effects of IL-4 after ICH. Collectively, these data confirm the importance of IL-4/STAT6/ST2 signaling in hematoma resolution and functional recovery after ICH. Intranasal IL-4 treatment warrants further investigation as a clinically feasible therapy for ICH.

intracerebral hemorrhage | microglia | macrophages | phagocytosis | bone marrow chimera

Intracerebral hemorrhage (ICH), a devastating form of stroke, occurs when blood extravasates into the brain parenchyma. Although ICH accounts for only 10 to 15% of all strokes in the United States, the mortality and morbidity in ICH patients exceeds that in ischemic stroke patients (1–4). Over 40% of ICH patients are dead by 1 y, and over 70% by 5 y (5–8). ICH is a growing epidemic; its incidence has increased worldwide by 47% over the past 20 y, especially in low- and middle-income countries (6). Current management options for ICH focus on the reduction of hematoma expansion and prevention of medical complications (9). Despite several randomized clinical trials, to date there are no medical or surgical therapies that significantly improve human functional outcome after ICH (10).

ICH leads to brain injury via primary and secondary mechanisms. Primary ICH injury is caused by the acute mass effect of the intracerebral hematoma, leading to brain tissue deformation/compression and elevated intracranial pressure. Hematoma size is a well-established biomarker for ICH severity and strongly predicts clinical outcomes (11). Recent data from the Minimally Invasive Surgery with Thrombolysis for Intracerebral hemorrhage Evacuation (MISTIE) III trial using minimally invasive surgery plus alteplase irrigation to treat ICH found that this form of intervention reduced mortality. Indeed, they observed that reducing ICH hematoma size could be associated with improved long-term outcome. Clot size reduction to 15 mL or less in the MISTIE group was associated with better neurological score (modified Rankin Scale) 1 y post-ICH, suggesting a threshold of procedure outcome that needs further evaluation in future trials (10). However, the invasive surgical removal of the ICH hematoma in many cases will not eliminate all blood in the brain parenchyma, due to the difficulty in determining the boundary of lesion and the possible diffuseness of the boundary. Nor will it stop the reaccumulation of blood at the lesion site if the hemorrhaging continues. In the international Surgical Trial in Intracerebral Hemorrhage (STICH) and the multicenter, randomized, controlled trial in the US on intraoperative stereotactic computed tomography-guided endoscopic surgery

Significance

Hemorrhagic stroke, resulting from intracerebral hemorrhage, is a devastating medical condition currently without effective cure. Here we report that intranasal delivery of IL-4, a well-known antiinflammatory cytokine, facilitates microglia- and macrophage-mediated hematoma resolution and improves long-term functional recovery in two different mouse models of intracerebral hemorrhage. Mechanistically, IL-4 activates a signaling cascade involving signal transducer and activator of transcription 6 and IL-1 receptor-like 1, thereby enhancing the phagocytotic capability of microglia and macrophages to remove red blood cells from intracerebral hematomata. Our in vitro and in vivo preclinical studies support the view that IL-4 treatment has the therapeutic potential to promote hematoma resolution and functional restoration in hemorrhagic stroke victims.

Author contributions: X.H., J.C., M.V.L.B., and G.C. designed research; J.X., Z.C., F.Y., H.L., C.M., and D.X. performed research; J.X., Z.C., F.Y., H.L., C.M., D.X., X.H., R.K.L., S.H.Y.C., R.A.S., Y.S., J.C., M.V.L.B., and G.C. analyzed data; F.Y., X.H., and J.C. wrote the paper; and J.X., Z.C., F.Y., H.L., C.M., D.X., X.H., R.K.L., S.H.Y.C., R.A.S., Y.S., J.C., M.V.L.B., and G.C. revised the manuscript.

Reviewers: C.B., University of South Florida; and H.S., University of California, San Francisco.

The authors declare no competing interest.

[1]J.X., Z.C. and F.Y. contributed equally to this work.

[2]To whom correspondence may be addressed. Email: michael.bennett@einstein.yu.edu or nju_neurosurgery@163.com.

This article contains supporting information online at https://www.pnas.org/lookup/suppl/doi:10.1073/pnas.2018497117/-/DCSupplemental.

First published December 8, 2020.

(ICES), early open, or endoscopic surgery to remove ICH hematoma did not improve functional recovery compared to medical management of ICH (12–14). All of these failures in clinical trials of hematoma evacuation suggest that mechanical hematoma removal is not enough to improve the ICH outcomes. Therefore, much attention has been paid to boost endogenous pathways for hematoma resolution/red blood cell (RBC) debris engulfment and to reduce secondary ICH injury.

Secondary ICH injury refers to the subacute and long-term injury due to oxidative stress, cerebral inflammation, perihematoma edema, mitochondrial dysfunction, and other detrimental factors (15). Although the detailed mechanisms of secondary injury after ICH remain elusive, some components of the blood within a hematoma are implicated as key factors mediating subacute and long-term brain damage. Early in its evolution, the hematoma is composed of erythrocytes (RBC), lysed RBC with debris, and scattered pools of plasma. The toxicity of erythrocyte-released hemoglobin (Hb) and Hb-derived heme and iron leads to neuronal loss, white matter injury, blood–brain barrier disruption, and functional decline after ICH (16, 17). Thus, accelerating and enhancing blood clearance and removal of RBC debris, including Hb and iron, is a legitimate therapeutic strategy for ICH.

Scavenger cells, such as CNS resident microglia and infiltrating macrophages, respond quickly to brain injuries, such as ICH, and engulf foreign substances and cell debris. Recruitment of microglia/macrophages to the site of bleeding has been observed as early as 1 h after intracerebral collagenase injection (18) and 4 h after blood injection (19, 20). One postmortem study revealed seven- to eightfold increases in the number of microglia/macrophages at the periphery of the hematoma within 5 to 10 d after acute ICH (21). The accumulation of microglia/macrophages persists for weeks after ICH (19, 20), suggesting that these phagocytes may influence both primary and secondary ICH injuries. The functions of microglia/macrophages in a hemorrhagic brain are diverse. They play critical roles in the clearance of blood from brain parenchyma, which reduces the deleterious mechanical effects of the hematoma and prevents cytotoxicity induced by components of the blood, including iron. Enhancement of the phagocytic function of microglia/macrophages has been shown to promote hematoma resolution, limit cerebral inflammation, reduce neuronal damage, and improve long-term neurological functions after ICH (22–25). Therefore, elucidating the mechanisms underlying microglia/macrophage-mediated phagocytosis may identify new therapeutic targets to improve ICH outcomes.

In this study, we identify signal transducer and activator of transcription 6 (STAT6) as a key enhancer of erythrocyte engulfment and removal in two established ICH models in mice. We report that activation of STAT6 by interleukin (IL)-4 after ICH promoted hematoma resolution, reduced brain injury, and improved long-term functional recovery. IL-1 receptor-like 1 (ST2) was important for the salutary effects of IL-4/STAT6 on hematoma clearance. Treatment with IL-4 or other STAT6 activators might therefore be worthy of further testing for the clinical management of ICH.

Results

IL-4 Treatment Improves Hematoma Resolution and Neurofunctional Recovery following ICH. In one model of ICH, blood collected from the donor mice of the same sex, age, and genetic background was stereotaxically injected into the right striatum of young adult (10-wk old) C57/BL6 male mice. Animals were then randomly assigned to receive administration of IL-4 nanoparticles (50 μg/kg body weight per day) or an equivalent volume of vehicle. IL-4 or vehicle was delivered intranasally 2 h after ICH and then once every 24 h for the next 7 d. We recently reported that a single intranasal administration of IL-4 nanoparticles increases IL-4 protein levels in the mouse brain for up to 24 h (26). Animals were scanned with 9.4 Tesla MRI successively on post-ICH days 1, 5, and 14 to monitor hematoma evolution and brain edema. Both T2- and T2*-weighted images were acquired and quantified by a blinded observer (27). While T2 is sensitive to free extracellular water and brain edema, T2* detects hematoma/iron deposition from paramagnetic deoxyhemoglobin, methemoglobin, or hemosiderin in hemorrhagic lesions (28, 29). Hemorrhagic brain lesions were observed as areas of hypointensity, which appeared to be black holes on the T2*-weighted images 1 d after ICH. The hypointense lesion areas gradually became heterogeneous lesions with both hyperintense (lighter than the surrounding tissues) and hypointense areas within the hematoma at day 5 to day 14 after ICH in vehicle-treated mice (Fig. 1*A*). Compared to vehicle-treated mice, IL-4 treatment had no effect on hematoma volume on T2* images at 1 d after ICH, but resulted in significant reduction or a strong trend of reduction in hematoma volume at 5 d ($P = 0.0859$) and 14 d ($P = 0.0085$) after ICH (Fig. 1*B*), respectively. The hematoma clearance was then calculated as a percentage by dividing the decrease in hematoma size by the starting hematoma size at 1 d after ICH in T2* images (Fig. 1*C*). Treatment with IL-4 significantly enhanced hematoma clearance by day 5 ($P = 0.003$) and day 14 ($P = 0.0355$), respectively, as compared to vehicle treatment (Fig. 1*C*). Thus, IL-4 treatment accelerates hematoma clearance after ICH.

T2-weighted images revealed overall changes in lesion sizes similar to T2* images from day 1 to day 14 after ICH (*SI Appendix*, Fig. S1*A*). IL-4–treated mice had significantly reduced brain edema at day 5 ($P = 0.0026$) (*SI Appendix*, Fig. S1*B*) and brain lesion volume at day 14 ($P = 0.0249$) (*SI Appendix*, Fig. S1*C*) after ICH, as compared to vehicle-treated mice.

The gross distribution of ICH was examined on freshly prepared thick brain slices 1, 5, and 7 d after blood injection (Fig. 1*D*). The hematoma volumes were reduced at 5 and 7 d, compared to 1 d, after blood injection in both the vehicle-treated group and IL-4–treated group. However, while IL-4 treatment had no effect on hematoma volumes at 1 d, it significantly reduced hematoma volumes at 5 d ($P = 0.0147$) and 7 d ($P = 0.0415$) after ICH compared to vehicle treatment (Fig. 1*D*). Blood contents in tissue homogenates of saline-perfused brains were also quantified using a spectrophotometric Hb assay (Fig. 1*E*). IL-4–treated mice had significantly reduced Hb contents at 5 d ($P = 0.0474$) and 7 d ($P = 0.0438$) after ICH compare to vehicle-treated mice. Histological iron staining demonstrated significantly decreased ferric iron deposition in IL-4–treated mice 14 d after ICH ($P = 0.0194$) compared to vehicle-treated mice (Fig. 1*F*). Together, the results of quantification of hematoma volume, Hb content, and iron deposition confirmed that post-ICH IL-4 treatment promotes hematoma clearance in the blood injection model.

Post-ICH IL-4 treatment significantly improved sensorimotor functions, as assessed by the adhesive removal test ($P = 0.0065$) (Fig. 1*G*), foot fault test ($P = 0.0242$) (Fig. 1*H*), and cylinder test ($P = 0.0288$) (Fig. 1*I*), over the course of 14 d after ICH. Spatial learning and memory performances, as assessed by the Morris water maze (MWM) test 16 to 21 d after ICH, were also significantly improved in IL-4–treated mice compared to vehicle-treated mice (learning phase, $P = 0.044$; memory phase, $P = 0.0143$) (Fig. 1*J*). Correlation analysis revealed that there were significantly positive correlations between the T2* hematoma volumes at 14 d after ICH and the sensorimotor functional deficits detected by either the adhesive removal test ($r = 0.6185$, $P = 0.0036$) (Fig. 1*K*) or cylinder test ($r = 0.4896$, $P = 0.0285$) (Fig. 1*L*). Moreover, there were significantly negative correlations between the T2*-determined hematoma clearance at day 5 after ICH and the sensorimotor functional deficits detected by the adhesive removal test at day 14 after ICH ($r = -0.5169$, $P = 0.0196$) (Fig. 1*M*). In contrast, a significantly negative correlation was not detected between the hematoma clearance at day 14

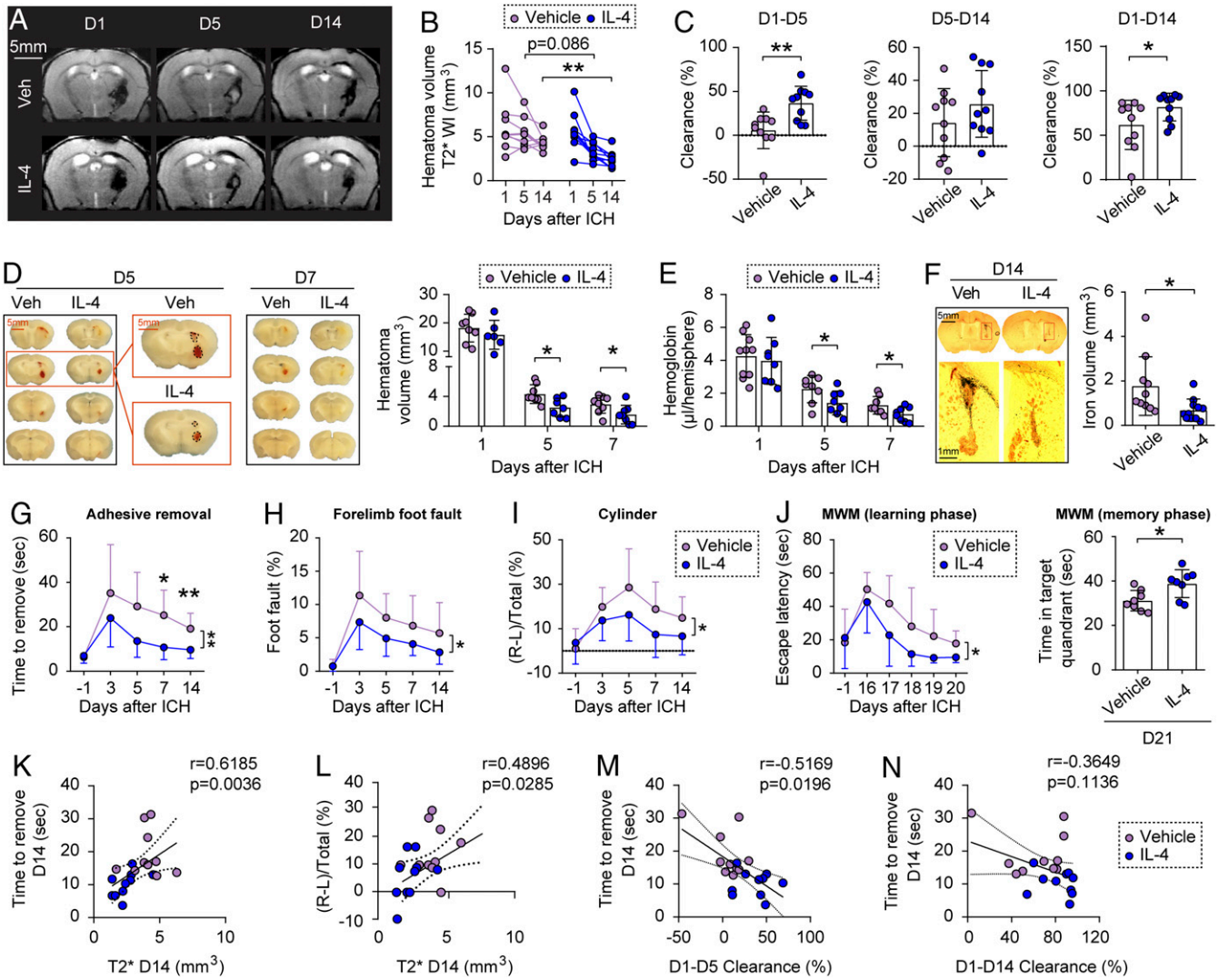

Fig. 1. IL-4 treatment improves hematoma resolution and neurofunctional recovery following ICH in young adult male mice. ICH was induced in 10-wk-old male C57/BL6 mice by blood injection into the right striatum, followed by intranasal IL-4 or vehicle nanoparticle treatment starting 2 h after ICH and repeated daily for the next 7 d. (*A*) Representative axial T2* images obtained from the same mouse in each group on days 1, 5, and 14 following ICH. (*B*) Quantification of hematoma volumes on T2*-weighted images. $n = 10$ per group. (*C*) Hematoma clearance was calculated on T2* images as the percentage decrease in hematoma size compared to the starting size. $n = 10$ per group. (*D*, *Left*) Representative serial coronal brain sections showing red-hued hematoma in IL-4 or vehicle-treated mice on day 5 or 7 after ICH. (*Right*) Quantification of hematoma volumes based on photographs of consecutive brain section at 1, 5, and 7 d after ICH. $n = 6$ to 8 per group. (*E*) Quantification of Hb content in the lesioned hemisphere at 1, 5, and 7 d after ICH. $n = 8$ to 10 per group. (*F*) Coronal brain sections stained for iron in IL-4 or vehicle-treated mice at 14 d after ICH. The red-boxed insets are higher-magnified views with hematoma outlined. Histogram shows quantification of iron$^+$ volume at 14 d after ICH. $n = 10$ to 11 per group. (*G–I*) Sensorimotor functions were measured by adhesive removal (*G*), foot fault (*H*), and cylinder (*I*) tests before (−1 d) and 3 to 14 d after ICH. $n = 9$ to 10 per group. (*J*) Spatial learning (*Left*) and memory (*Right*) were assessed by the MWM before surgery (−1 d) and 16 to 21 d after ICH. $n = 8$ mice per group. $^*P < 0.05$, $^{**}P < 0.01$ by Student's *t* test (*C*, *F*, and *J*) Mann–Whitney *U* test (*C*), or by two-way repeated measures ANOVA and Bonferroni post hoc tests (*B*, *G*, and *J*). The asterisks at the right indicate the group differences. The asterisks on the top indicate single day comparison between the two groups. (*K*) Spearman correlation analysis between the performance in adhesive removal test and T2* imaging-based hematoma volumes 14 d after ICH. (*L*) Pearson correlation analysis between the performance in cylinder test and T2* imaging-based hematoma volumes 14 d after ICH. (*M* and *N*) Spearman correlation analysis between the performance in adhesive removal test 14 d after ICH and MRI assessments of hematoma clearance at 1 to 5 d (*M*) or 1 to 14 d (*N*) after ICH.

after ICH and the adhesive removal test at day 14 after ICH ($r = -0.3649$, $P = 0.1136$) (Fig. 1*N*).

To better mimic the clinical scenario, we tested the therapeutic effect of IL-4 after ICH in aged (18-mo old) male mice and young (10-wk old) female mice. Aged male mice exhibited greater neurofunctional deficits after ICH in the adhesive removal test, foot fault test, and cylinder test (*SI Appendix*, Fig. S2 *A–C*), as compared to young male mice (Fig. 1 *G–I*). Nevertheless, IL-4 treatment significantly ameliorated sensorimotor deficits after ICH in the aged mice in all three tests (*SI Appendix*, Fig. S2 *A–C*). Young female mice performed sensorimotor functions similarly as young males after ICH, and IL-4 treatment significantly improved the performance by female mice in the adhesive removal test and foot fault test, but not in the cylinder test after ICH (*SI Appendix*, Fig. S2 *D–F*).

IL-4 Treatment Accelerated STAT6 Activation in Microglia/Macrophages after ICH. STAT6 is a transcription factor that lies downstream of IL-4 signal transduction (30). Therefore, we examined the activation of STAT6 after ICH induced by blood injection using a

phospho-specific antibody (Tyr641) that recognizes the phosphorylated, active form of STAT6 (pSTAT6). Previous studies revealed that microglia/macrophages begin to accumulate at the edges of the hematoma early after ICH (19, 20), and there were very few microglia/macrophages within the hematoma core (21). We also found here that microglia/macrophages, which are positive for ionized calcium binding adaptor molecule 1 (Iba1), accumulated at the edges of hematoma with very little penetration into the core (*SI Appendix*, Fig. S3*A*). pSTAT6 immunofluorescence was barely detectable in sham control brain; however, it was robustly enhanced in Iba1$^+$ cells 3 to 7 d after ICH, peaking at 5 d after ICH (*SI Appendix*, Fig. S3 *A* and *B*). Flow cytometry analyses conducted at 3 d after ICH confirmed the markedly elevated pSTAT6 immunofluorescence in CD45$^+$CD11b$^+$ microglia/macrophages (*SI Appendix*, Fig. S3*C*), which was in contrast to baseline levels of pSTAT6 immunofluorescence in other CNS cells, such as astrocytes (CD45$^-$GLAST$^+$), oligodendrocytes (CD45$^-$O4$^+$), and neurons (CD45$^-$NeuN$^+$) (*SI Appendix*, Fig. S3*C*). Compared to vehicle controls, IL-4 treatment significantly increased pSTAT6 immunofluorescence in Iba1$^+$ cells at 1 d ($P = 0.0198$) and 3 d ($P = 0.0286$) after ICH induced by blood injection (*SI Appendix*, Fig. S3 *D* and *E*). These results suggest that IL-4 treatment hastens STAT6 activation mainly in microglia and macrophages after ICH.

We also observed activation of STAT6 in the collagenase injection model of ICH, where expression of pSTAT6 was elevated 3 to 14 d after ICH (*SI Appendix*, Fig. S3 *F* and *G*). Immunofluorescent staining confirmed no obvious pSTAT6 signal in NeuN$^+$ neurons, glial fibrillary acidic protein (GFAP)$^+$ astrocytes, or adenomatous polyposis coli (APC)$^+$ oligodendrocytes after ICH (*SI Appendix*, Fig. S3*H*). These observations again suggest the activation of STAT6 in microglia/macrophages during the subacute stages after ICH.

STAT6 Promotes Hematoma Resolution and Neurofunctional Recovery after ICH in the Blood Injection Model. To further determine the role of STAT6 in ICH outcomes, adult male WT and STAT6 knockout (KO) mice were subjected to blood injection, respectively. Longitudinal T2*-weighted MRI scanning revealed significantly enlarged hematoma and iron deposition volumes during the delayed injury phase after ICH in STAT6 KO mice ($P = 0.043$ and $P = 0.014$ at 5 and 14 d, respectively) compared to WT mice (Fig. 2 *A* and *B*). IL-4 treatment in STAT6 KO mice tended to reduce hematoma volumes (from 8.862 ± 3.322 mm^3 to 6.575 ± 1.176 mm^3 at 5 d; from 6.449 ± 1.829 mm^3 to 5.353 ± 1.150 mm^3 at 14 d); however, neither of the differences reached statistical significance ($P = 0.313$ and $P = 0.587$ at 5 and 14 d, respectively). Ferric iron deposition volumes were quantified on consecutive brain sections stained for iron at 14 d after ICH. STAT6 KO mice exhibited a significantly enlarged iron deposition volume compared to WT mice, reflecting a delayed iron clearance, and this delay in STAT6 KO mice could not be reversed by IL-4 treatment (Fig. 2*C*). Neither STAT6 KO nor IL-4 treatment in STAT6 KO mice had significant effects on brain lesion volume detected by T2-weighted images (*SI Appendix*, Fig. S4 *A* and *B*). As expected, the amount of iron deposition strongly correlated with the brain lesion size on T2*-weighted ($r = 0.7825$, $P = 0.0001$) (*SI Appendix*, Fig. S4*C*), but not T2-weighted images ($r = 0.3283$, $P = 0.1836$) (*SI Appendix*, Fig. S4*D*), suggesting that T2* imaging of hematoma/iron deposition is superior to T2 imaging for detection of injury in the ICH model. These results suggest a role for STAT6 in facilitating hematoma and iron clearance after ICH. Nevertheless, IL-4–treated STAT6 KO mice no longer showed significantly increased hematoma and iron deposition volume after ICH compared to WT mice (Fig. 2 *B* and *C*), indicating that IL-4 may promote hematoma resolution through both STAT6-depedent and -independent mechanisms.

Sensorimotor functions were evaluated by the adhesive removal test (Fig. 2*D*) and foot fault test (Fig. 2*E*) for 14 d after

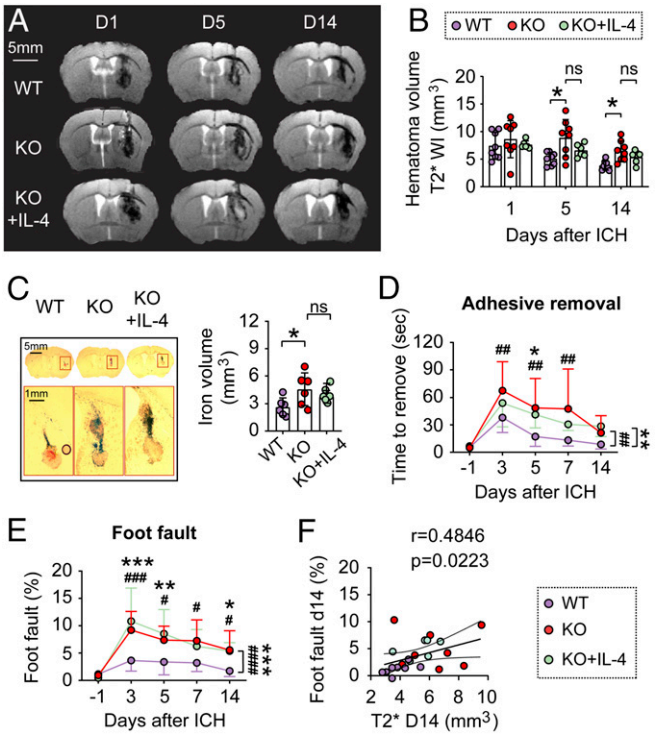

Fig. 2. STAT6 promotes hematoma resolution and neurofunctional recovery after ICH in the blood-injection model. ICH was induced in WT and STAT6 KO mice by blood injection into the right striatum. IL-4 nanoparticles were intranasally applied starting 2 h after ICH and this was repeated daily for the next 7 d. (*A*) Representative T2* images obtained from the same mouse in each group at 1, 5, and 14 d after ICH. (*B*) Quantification of hematoma volumes on T2*-weighted images at 1, 5, and 14 d after ICH. $n = 6$ to 8 per group. Note that STAT6 KO mice had significantly larger hematoma volumes compared to WT mice at 5 and 14 d after ICH; meanwhile IL-4 treatment failed to significantly reduce hematoma volumes in STAT6 KO mice. (*C*, *Left*) Coronal brain sections stained for iron deposition at 14 d after ICH. (*Right*) Quantification of iron$^+$-staining volume. $n = 6$ per group. (*D* and *E*) Sensorimotor functions were assessed by adhesive removal (*D*) and foot fault (*E*) tests before surgery (−1 d), and 3 to 14 d after ICH. $n = 6$ to 8 per group. (*F*) Spearman correlation analysis between foot fault behavior test and T2* imaging-based hematoma volumes at 14 d after ICH. ns, not significant; $^*P < 0.05$, $^{**}P < 0.01$, $^{***}P < 0.001$ KO vs. WT, $^{\#}P < 0.05$, $^{\#\#}P < 0.01$, $^{\#\#\#}P < 0.001$, $^{\#\#\#\#}P < 0.0001$ KO+IL-4 vs. WT, by one-way ANOVA and Tukey post hoc tests (*C*) or by two-way repeated measures ANOVA (*B*, *D*, and *E*) and Bonferroni post hoc tests. The asterisks/pound signs at the right indicate the group differences. The asterisks/pound signs on the top indicate single day comparison between the two groups.

ICH, in which STAT6 KO mice demonstrated exacerbated neurological deficits after ICH compared to WT mice. IL-4 treatment failed to improve the sensorimotor performances by STAT6 KO mice (Fig. 2 *D* and *E*). Spearman correlation analysis revealed that the sensorimotor functional deficits detected by the foot fault test significantly correlated with the T2* hematoma volumes 14 d after ICH ($r = 0.4846$, $P = 0.0223$) (Fig. 2*F*).

Deterioration of sensorimotor functions after ICH was also observed in STAT6 KO female mice compared to WT female mice using adhesive removal and cylinder tests (*SI Appendix*, Fig. S4*E*), indicating that STAT6 contributes to neurofunctional recovery after ICH in both sexes.

STAT6 Promotes Hematoma Resolution and Neurofunctional Recovery after ICH in the Collagenase Injection Model. We also determined the role of STAT6 in hematoma resolution and neurological recovery after ICH using the collagenase injection model. Type

VII-S collagenase (0.05 U in 1 μL of TESCA buffer) was injected into the right-side striatum of age- and body weight-matched male mice, which resulted in brain hematoma with comparable sizes in WT and STAT6 KO mice within 24 h after injection (Fig. 3 *A* and *B*). However, hematoma volume (Fig. 3 *A* and *B*) and Hb content (Fig. 3*C*), respectively, were significantly larger in the brain of STAT6 KO mice 5 and 7 d after ICH compared to WT mice. These results suggested an impaired hematoma resolution in STAT6 KO mice.

Long-term sensorimotor and spatial cognitive functions were assessed in collagenase-injected mice and sham controls using the rotarod test (Fig. 3*D*) and MWM test (Fig. 3 *E*–*H*) up to 11 d and 21 d, respectively, after collagenase or vehicle (sham) injection. Consistent with the observations on the blood-injection model, STAT6 KO mice demonstrated significantly exacerbated sensorimotor performance deficits (Fig. 3*D*) and spatial learning and memory impairments (Fig. 3 *E*–*H*) after ICH compared to WT mice.

Critical Role of STAT6 in Erythrophagocytosis by Microglia and Macrophages In Vivo and In Vitro. Massive accumulation of $Iba1^+$ microglia/macrophages surrounding the iron deposit (iron-staining$^+$) was readily detected 14 d after blood injection (Fig. 4*A*). The close proximity of microglia/macrophages to the iron deposit was consistent with the role for these phagocytes in hematoma clearance. The observed impairment of hematoma resolution after ICH in STAT6 KO mice prompted us to further explore its role in blood clearance by microglia and macrophages. To this end, RBCs in blood were fluorescently labeled and stereotaxically injected into the right striatum, and mice were killed 3 d after RBC injection. Single-cell striatal suspensions were prepared and stained with antibodies recognizing lymphocyte antigen 6 complex locus G6D (Ly6G, a marker of neutrophils), CD45, and CD11b, and subjected to FACS. Cells with intermediate (int) and high (hi) expression levels of CD45, including $Ly6G^-CD45^{int}CD11b^+$ resting microglia and $Ly6G^-CD45^{hi}CD11b^+$ macrophages/activated microglia were identified, respectively (Fig. 4*B*). Quantitatively, the numbers of activated phagocytes engulfing fluorescently labeled RBCs (recognized as $RBC^+Ly6G^-CD45^{hi}CD11b^+$) were significantly lower ($P = 0.0087$) (Fig. 4*C*) in STAT6 KO (18.08 ± 11.89% of total $Ly6G^-CD45^{hi}CD11b^+$ cells) than WT (40.67 ± 16.2% of total $Ly6G^-CD45^{hi}CD11b^+$ cells) mice. The numbers of $RBC^+Ly6G^-CD45^{int}CD11b^+$ microglia were also moderately decreased in STAT6 KO (3.15 ± 2.612% of total $Ly6G^-CD45^{int}CD11b^+$ cells) than WT (4.7 ± 0.92% of total $Ly6G^-CD45^{int}CD11b^+$ cells) mice, although the difference was not statistically significant ($P = 0.2004$) (Fig. 4*D*). These results suggest that in post-ICH brain the majority of resting microglia (>90%) are not active phagocytes for RBCs, whereas ~40% of macrophages/activated microglia participate in blood clearance.

We then evaluated the effect of STAT6 KO on the phagocytotic capacities of microglia and macrophages using primary cultures. Microglia or macrophages derived from STAT6 KO mice and WT mice were incubated with fluorescently labeled RBCs, respectively, and the engulfment of RBCs was quantified by FACS 2 h after incubation (Fig. 4*E*). STAT6-deficient microglia and macrophages exhibited significantly reduced RBC phagocytosis compared to respective WT controls (Fig. 4 *F* and *G*). Immunofluorescent staining of primary microglial cultures confirmed the reduced phagocytotic capacity for RBCs of STAT6 KO cells compared to WT cells. The percentages of

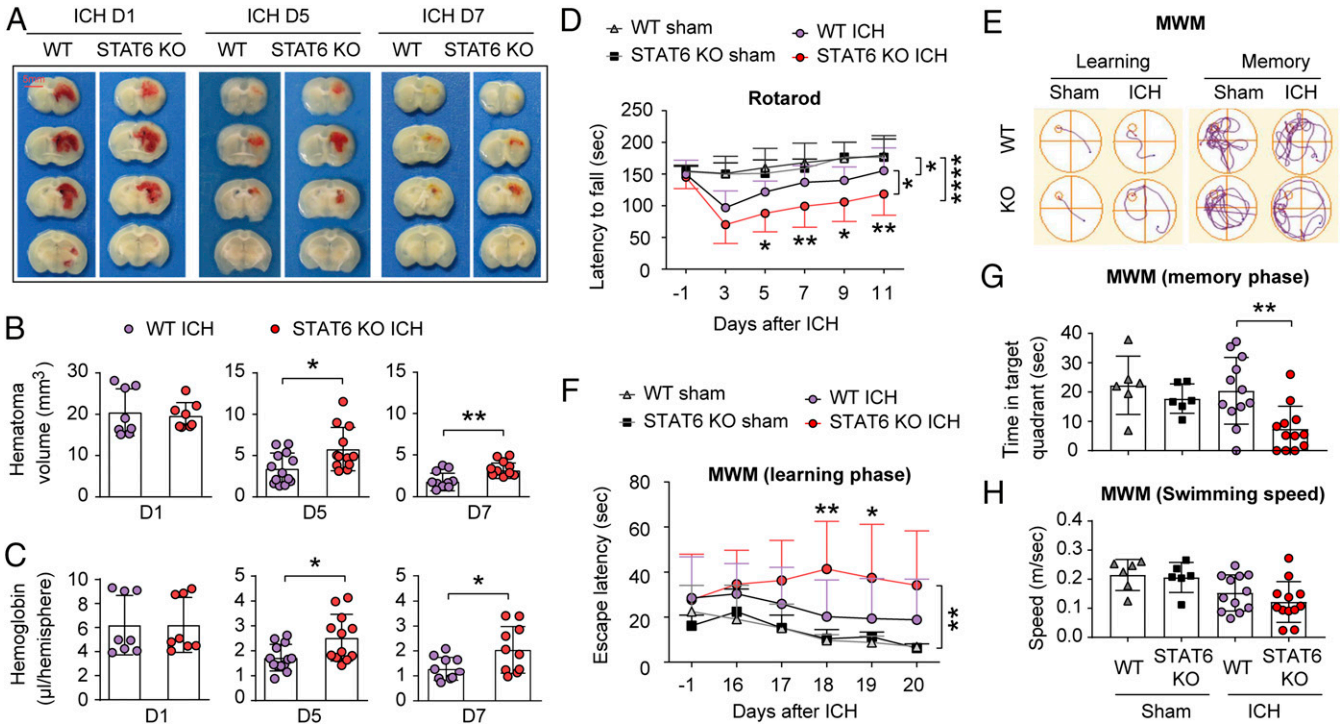

Fig. 3. STAT6 promotes hematoma resolution and neurofunctional recovery after ICH in the collagenase-injection model. ICH was induced in WT and STAT6 KO mice by collagenase (0.05 U) injection into the right striatum. (*A*) Representative coronal brain sections showing the red-hued hematoma in WT or STAT6 KO mice at 1, 5, and 7 after ICH. (*B*) Quantification of hematoma volumes on images in *A*. $n = 8$ to 13 per group. (*C*) Quantification of Hb contents in the lesioned hemisphere at 1, 5, and 7 d after ICH. $n = 8$ to 13 per group. (*D*) Sensorimotor functions were assessed by the rotarod test before surgery (−1 d) and 3 to 11 d after ICH. $n = 6$ for sham groups and $n = 12$ for ICH groups. (*E*–*H*) Spatial learning (*E* and *F*) and memory (*G*) were assessed by the MWM at 16 to 20 and 21 d after ICH, respectively. Similar swim speeds were observed among groups (*H*). $n = 6$ for sham groups and $n = 12$ for ICH groups. $^*P < 0.05$, $^{**}P < 0.01$, $^{****}P < 0.0001$ by Student's *t* test (*B* and *C*), one-way ANOVA (*G* and *H*), or two-way repeated measures ANOVA and Bonferroni post hoc tests (*D* and *F*). The asterisks at the right indicate the group differences. The asterisks on the top indicate single day comparison between the two groups.

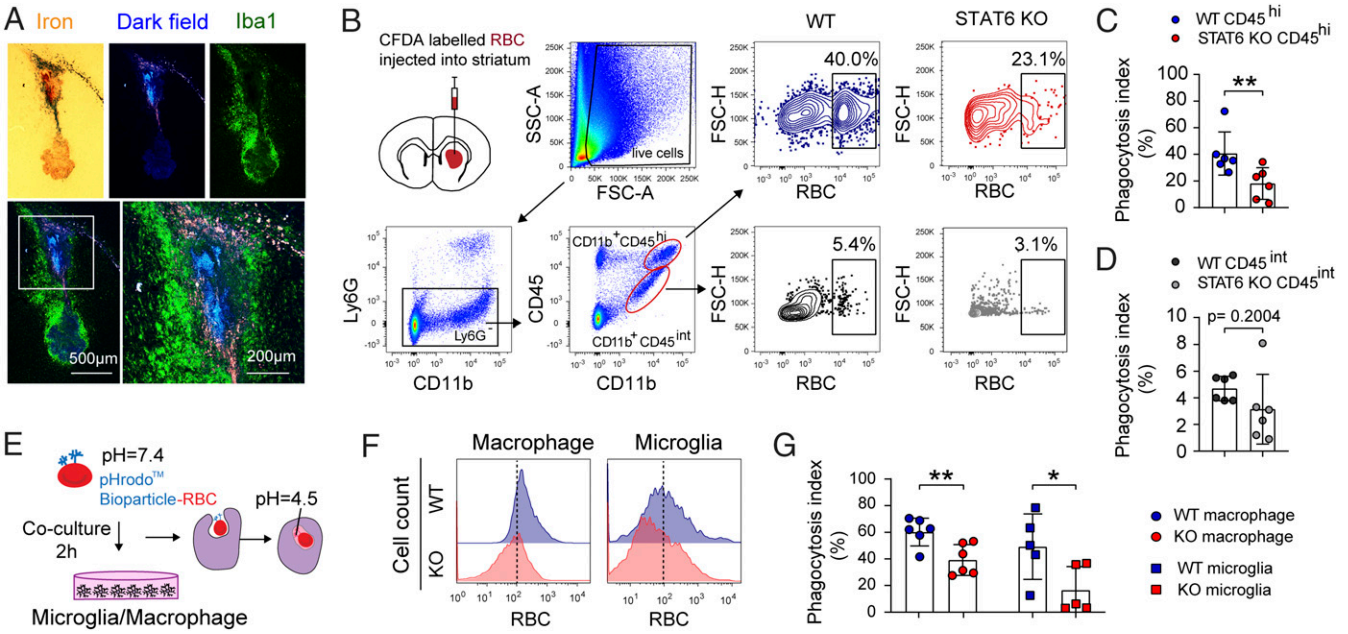

Fig. 4. STAT6 is required for erythrophagocytosis by microglia and macrophages in vivo and in vitro. (*A*) Microglia/macrophages (Iba1$^+$, green) were accumulated near the iron deposit (pink and blue under dark field) at 14 d after ICH. (*B*) RBCs were labeled with fluorescent dye and then injected into the right striatum of WT or STAT6 KO mice. Flow cytometry analysis, performed at 3 d after RBC injection, demonstrated that RBCs were engulfed by Ly6G$^-$CD45^{int}CD11b$^+$ resting microglia and Ly6G$^-$CD45^{hi}CD11b$^+$ macrophages/activated microglia. FSC-A, forward scatter-area; FSC-H, forward scatter-height; Ly6G: lymphocyte antigen 6 complex locus G6D, a marker of neutrophils; SSC-A, side scatter-area. (*C*) Quantification of RBC phagocytosis by activated microglia and macrophages. RBC$^+$ cells were recognized as phagocytotic cells. Data (phagocytosis indices) were expressed as percentage of Ly6G$^-$CD45^{hi}CD11b$^+$ cells that contain RBCs. $n = 6$ per group. (*D*) Quantification of RBC phagocytosis as percentage of Ly6G$^-$CD45^{int}CD11b$^+$ resting microglia containing RBCs. $n = 6$ per group. (*E–G*) RBCs were labeled with fluorescent dye and then incubated with primary cultures of microglia or macrophages for 2 h. (*E*) Experimental design. (*F*) Flow cytometry analysis of RBC-engulfing microglia and macrophages 2 h after incubation with labeled RBCs. Dashed lines show the gating for positive cell populations based on the position of fluorescence minus one controls. (*G*) Quantification of RBC-engulfing microglia and macrophages 2 h after incubation with labeled RBCs. $n = 5$ to 6 per group. Data were expressed as percentage of cells that contain RBCs; $^*P < 0.05$, $^{**}P < 0.01$ vs. WT by Mann–Whitney *U* test (*C*) or Student's *t* test (*D* and *G*).

microglia containing RBCs were less in cultures from STAT6-deficient microglia than in WT microglia 0.5 to 4 h after RBC-microglia coculture (*SI Appendix*, Fig. S5).

STAT6 Tempers Neuroinflammatory Reactions in Microglia and Macrophages after ICH. Activated microglia and macrophages may release toxic proinflammatory mediators and free radicals during hematoma resolution, leading to secondary brain injury in neighboring cells. Therefore, we evaluated the effect of STAT6 KO on inflammatory responses in microglia and macrophages after ICH. Flow cytometry was performed 5 d after blood injection in STAT6 KO mice and WT mice. The results revealed that the numbers of CD45^{hi}CD11b$^+$ cells (macrophages/activated microglia) were significantly increased in STAT6 KO mice compared to WT mice after ICH ($P = 0.0008$) (Fig. 5*A*), while the numbers of CD45^{int}CD11b$^+$ cells (resting microglia) were comparable between STAT6 KO and WT mice ($P = 0.2203$) (Fig. 5*B*). We further evaluated the protein levels of a panel of inflammation-regulatory cytokines in CD45^{hi}CD11b$^+$ and CD45^{int}CD11b$^+$ populations 5 d after ICH. The levels of anti-inflammatory markers, arginase 1 (Arg1) and IL-4, were significantly decreased ($P = 0.0486$ for Arg1; $P = 0.0396$ for IL-4) in CD45^{hi}CD11b$^+$ cells (Fig. 5 *C* and *E*), but not in CD45^{int}CD11b$^+$ cells (Fig. 5 *D* and *F*), of STAT6 KO mice compared to WT mice. In contrast, the levels of proinflammatory markers, including IL-6 and TNF-α, were not significantly different in either cell population between STAT6 KO and WT mice.

STAT6-Competent Microglia and Macrophages Promote Neurological Recovery after ICH. To determine whether both microglia and infiltrating macrophages contribute to hematoma resolution after ICH, we constructed reporter-chimera mice by transferring the bone marrow of CX3CR1 (micrglia/macrophage promoter)-GFP mice to bone marrow-depleted (irradiated head-shielded) WT mice (Fig. 6*A*). These reporter-chimera mice thus had GFP$^-$ residential microglia and GFP$^+$ peripheral macrophages. We observed both infiltrated GFP$^+$ macrophages and GFP$^-$ microglia among the Iba1$^+$ populations in the perihematoma areas 7 d after ICH (Fig. 6 *B* and *C*), but the GFP$^+$Iba1$^+$ macrophages appeared to significantly outnumber the GFP$^-$Iba1$^+$ microglia ($P = 0.0003$) (Fig. 6 *B* and *C*). Only GFP$^-$Iba1$^+$ microglia were observed in the contralateral non-ICH hemisphere (Fig. 6*C*).

To determine the relative importance of STAT6 expression in resident microglia and infiltrating peripheral macrophages to ICH outcomes, we constructed three types of chimera by bone marrow transfer to irradiated head-shielded mice (Fig. 6*D*): 1) WT bone marrow transferred to WT recipients (WT/WT); 2) STAT6 KO bone marrow transferred to WT recipients (WT/KO); 3) WT bone marrow transferred to STAT6 KO recipients (KO/WT). The absence of STAT6 in either microglia (KO/WT) or peripheral cells (WT/KO) significantly worsened sensorimotor performance in the rotarod test (Fig. 6*E*). The KO/WT and WT/KO chimera mice also showed significantly greater iron deposition in the ICH brain than WT/WT mice (Fig. 6*F*), but there was no significant difference between WT/KO and KO/WT chimera mice ($P = 0.0937$). These results suggest that STAT6 activation in both CNS microglia and peripheral cells contribute to neurological recovery after ICH.

To further determine the role of STAT6 as a key signaling mechanism underlying macrophage-afforded protection against ICH, we reasoned that adoptive transfer of STAT6-competent

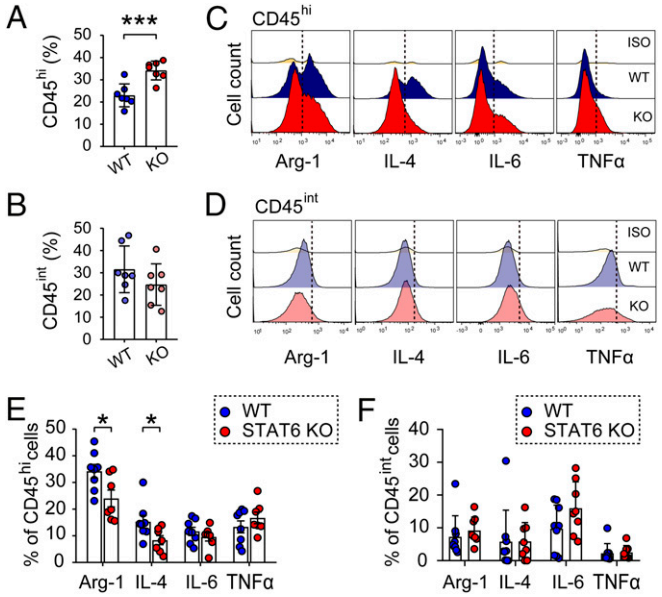

Fig. 5. STAT6 tempers neuroinflammatory reactions in microglia and macrophages after ICH. ICH was induced in WT and STAT6 KO mice by blood injection into the right striatum, and mice were killed 5 d after ICH. (*A* and *B*) Quantification of $CD45^{hi}CD11b^{+}$ macrophages/activated microglia (*A*) and $CD45^{int}CD11b^{+}$ resting microglia (*B*) as percentages per total number of single cells in each brain. (*C* and *D*) Flow cytometry was used to assess the expression of phenotypic markers by microglia/macrophages in the ICH brain. Representative flow cytometry plots showing the expression of Arg1, IL-4, IL-6, and TNF-α expression in $CD45^{hi}CD11b^{+}$ macrophages/activated microglia (*C*) and in $CD45^{int}CD11b^{+}$ resting microglia (*D*). (*E* and *F*) The expression of neuroinflammation associated markers were expressed as percentages of specific marker positive cells per total number of $CD45^{hi}CD11b^{+}$ macrophages/activated microglia (*E*) or $CD45^{int}CD11b^{+}$ resting microglia (*F*). Iso: Rabbit IgG as an isotype control. Dashed lines show the gating for positive cell populations based on the position of fluorescence minus one controls. $n = 7$ to 9 per group. $^{*}P < 0.05$, $^{***}P < 0.001$ STAT6 KO vs. WT by Student's *t* test (*A*, *B*, and *E*) or by Mann–Whitney *U* test (*F*).

macrophages might be able to rescue the poorer ICH outcomes in STAT6 KO mice. To this end, we intravenously infused WT or STAT6-deficient macrophages (2×10^6 cells per mouse) to STAT6 KO mice 2 h after blood injection (Fig. 7*A*), resulting in KO/KO (KO mice/containing KO macrophages) and KO/WT (KO mice/containing WT macrophages) mice, respectively. MRI T2* scanning demonstrated that post-ICH infusion with WT macrophages significantly reduced brain lesion sizes 5 d ($P = 0.0279$) and 14 d ($P = 0.0083$) after ICH, as compared to STAT6 KO macrophages-infused mice (Fig. 7*B*). Compared to STAT6 macrophage-infused mice, WT macrophage infused mice showed significantly facilitated hematoma clearance at day 5 (KO/WT 21.59 ± 21.91% vs. KO/KO −1.174 ± 7.942%, $P = 0.0378$) and day 14 (KO/WT 44.40 ± 8.1% vs. KO/KO 15.69 ± 8.91%, $P = 0.0002$) after ICH (Fig. 7*C*). Results of iron staining performed on the same set of brains underwent MRI T2* scanning demonstrated that WT macrophage infusion significantly ameliorated iron brain deposition 14 d after ICH in STAT6 KO mice (Fig. 7*D*). Taken together, the results confirmed the critical role of STAT6 in macrophage-afforded hematoma clearance after ICH.

Sensorimotor functions were assessed using the adhesive removal (Fig. 7*E*) and foot fault (Fig. 7*F*) tests for 14 d after ICH in KO/KO and KO/WT mice, respectively. The KO/WT mice exhibited significantly better sensorimotor performance in both tests after ICH compared to KO/KO mice (adhesive removal, $P = 0.0131$; foot fault, $P = 0.0062$, KO/WT vs. KO/KO mice). Pearson correlation analyses revealed that while the performance in the adhesive removal test was not significantly correlated with the T2* hematoma clearance during the first 5 d ($r = -0.1608$, $P = 0.6192$) (Fig. 7*G*), there were strong correlations between the adhesive removal test and the T2* hematoma size ($r = 0.5909$, $P = 0.043$) (Fig. 7*H*) and between the adhesive removal test and the T2* hematoma clearance ($r = -0.6537$, $P = 0.0211$) (Fig. 7*I*) at 14 d after ICH.

ST2 as a Signaling Molecule Downstream of STAT6 in Facilitating Hematoma Resolution after ICH. Given that STAT6 is a transcription factor promoting phagocytotic activity of microglia and macrophages after ICH, we explored phagocytosis-specific genes downstream of STAT6 regulation. To this end, we performed quantitative PCR arrays to analyze the expression levels of 90 phagocytosis-relevant genes using FACS-purified $CD45^{hi}CD11^{+}$

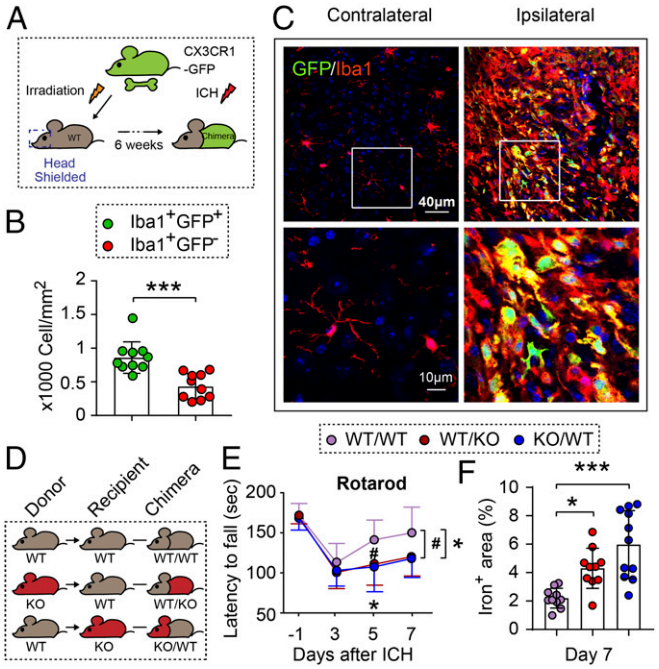

Fig. 6. Induction of ICH in chimeric mice: STAT6-competent microglia and macrophages promote hematoma resolution and neurological recovery. (*A*) Schematic illustration for the construction of WT/CX3CR1-GFP (CX3 chemokine receptor 1/green fluorescent protein) chimeric mice. WT recipients were subjected to irradiation (950 rad) with their heads shielded, and 6 h later received bone marrow transplantation from CX3CR1-GFP donors. WT/CX3CR1-GFP chimeric mice with GFP^{-} CNS microglia and GFP^{+} peripheral immune cells were subjected to collagenase injection into the right striatum 6 wk after chimeric construction. (*B*) Quantification of the number of $GFP^{+}Iba1^{+}$ macrophages and $GFP^{-}Iba1^{+}$ microglia in perihematoma regions as indicated in *C*. $n = 10$ per group. $^{***}P < 0.001$ by Student's *t* test. (*C*) Representative images showing that both $GFP^{+}Iba1^{+}$ macrophages and $GFP^{-}Iba1^{+}$ microglia were accumulated around the hematoma 7 d after ICH. (*D*) Chimeric mice were constructed by transplanting WT bone marrow to WT recipients (WT/WT), STAT6 KO bone marrow to WT recipients (WT/KO), or WT bone marrow to STAT6 KO recipients (KO/WT) after irradiation of the head shielded recipients. Chimeric mice were subjected to collagenase injection into the right striatum 6 wk after chimeric construction. (*E*) Sensorimotor function was assessed by the rotarod test before surgery (−1 d) and 3 to 7 d after ICH. $n = 10$ to 11 per group. (*F*) Quantification of iron^{+} volume 7 d after ICH. $n = 9$ to 11 per group. $^{*}P < 0.05$ (WT/KO vs. WT/WT) or $^{\#}P < 0.05$ (KO/WT vs. WT/WT) by two-way repeated measures ANOVA (*E*) or $^{*}P < 0.05$; $^{***}P < 0.001$ vs. WT/WT by one-way ANOVA (*F*) and Bonferroni post hoc tests. The asterisks/pound symbols at the right indicate the group differences. The asterisks/pound symbols on the top indicate single day comparison between the two groups.

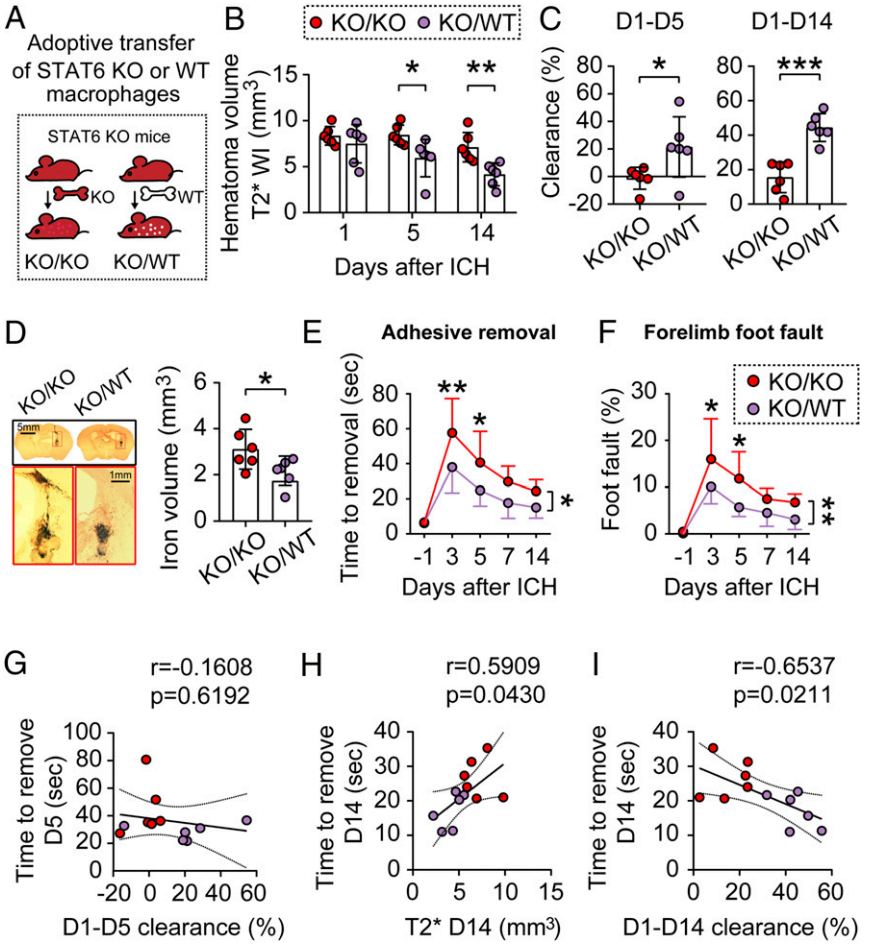

Fig. 7. Adoptive transfer of STAT6-competent macrophages improves outcomes after ICH in STAT6 KO mice. ICH was induced in STAT6 KO mice by blood injection into the right striatum. (*A*) Two million macrophages prepared from either WT mice or STAT6 KO mice were adoptively transferred (intravenous route) into the STAT6 KO mice 2 h after ICH. (*B*) Quantification of hematoma volumes on T2*-weighted images at 1, 5, and 14 d after ICH. $n = 6$ per group. (*C*) Hematoma clearance was calculated on T2* images as the percentage decreases in hematoma size compared to the starting size on day 1. $n = 6$ per group. (*D*, *Left*) Coronal brain sections stained for iron deposition 14 d after ICH. (*Right*) Quantification of iron$^+$ volume. $n = 6$ per group. (*E* and *F*) Sensorimotor functions were assessed by the adhesive removal (*E*) and foot fault (*F*) tests before surgery (−1 d) and 3 to 14 d after ICH. $n = 6$ per group. $^*P < 0.05$, $^{**}P < 0.01$, $^{***}P < 0.001$ by Student's *t* test (*C* and *D*) or by two-way repeated measures ANOVA and Bonferroni post hoc tests (*B*, *E*, and *F*). The asterisks at the right indicate the group differences. The asterisks on the top indicate single day comparison between the two groups. (*G*) Pearson correlation analysis between the functional performance in adhesive removal test and the hematoma clearance 5 d after ICH. (*H* and *I*) Pearson correlation analysis between the functional performance in adhesive removal test and the hematoma volumes in T2*-weighted imaging 14 d after ICH (*H*) or the hematoma clearance 14 d after ICH (*I*).

cells (macrophages and activated microglia) from WT and STAT6 KO brains (hemispheres ipsilateral to the ICH side), respectively, 5 d after ICH (Fig. 8*A*). Three such genes were significantly up-regulated (*Colec12*, 1.946 ± 0.035 fold vs. WT, $P = 0.007$; *Cd36*, 1.791 ± 0.221 fold vs. WT, $P = 0.0174$; *Ticam*, 1.341 ± 0.03 fold vs. WT, $P = 0.0139$) and three such genes were significantly down-regulated (*Il1rl1*, 0.535 ± 0.131 fold vs. WT, $P = 0.0478$; *Cnn2*, 0.453 ± 0.085 fold vs. WT, $P = 0.0047$; *Fcer1g*, 0.545 ± 0.028 fold vs. WT, $P = 0.0471$) in STAT6 KO brains compared to WT brains (Fig. 8*B*).

Among the down-regulated genes in STAT6 KO post-ICH mice, *Il1rl1* encodes the ST2 protein, a member of the IL-1 receptor superfamily known to be essential for phagocytosis by phagocytes (31). Therefore, we further determined the role of ST2 as a potential prophagocytosis molecule downstream of STAT6 regulation. First, immunofluorescent staining was performed to detect ST2 expression 5 d after ICH. As shown (Fig. 8*C*), ST2 immunofluorescence was detectable in few cells in the contralateral hemisphere of ICH brain of either WT or STAT6 KO mice; however, ST2 immunofluorescence was markedly up-regulated in the perihematoma regions of ipsilateral hemisphere in ICH brain. Approximately 50% of ST2$^+$ cells were Iba1$^+$ microglia and macrophages. The numbers of ST2$^+$Iba1$^+$ cells were significantly lower in STAT6 KO mice than WT mice (19.89 ± 9.242/mm^2 KO vs. 103.5 ± 43.5/mm^2 WT, $P = 0.001$). Second, we determined the role of ST2 in hematoma clearance and neurofunctional outcomes by inducing ICH in ST2 KO mice and WT mice, respectively. Hematoma volumes were significantly larger in ST2 KO mice than WT mice 5 d after ICH ($P = 0.0332$) (Fig. 8*D*). Sensorimotor deficits in both foot fault ($P = 0.0120$) and cylinder tests ($P = 0.0129$) were significantly exacerbated in ST2 KO mice compared to WT mice 1 to 5 d after ICH (Fig. 8*E*). Third, in the same set of experiments, we determined whether post-ICH intranasal delivery of IL-4 nanoparticles could rescue the poorer outcomes exhibited by ST2 KO mice. IL-4 treatment failed to significantly reduce hematoma volumes (Fig. 8*D*) or improve sensorimotor performance in ST2 KO mice (Fig. 8*E*). Finally, Spearman correlation analysis revealed that there was strong positive correlation between the cylinder test and hematoma volume among the 3

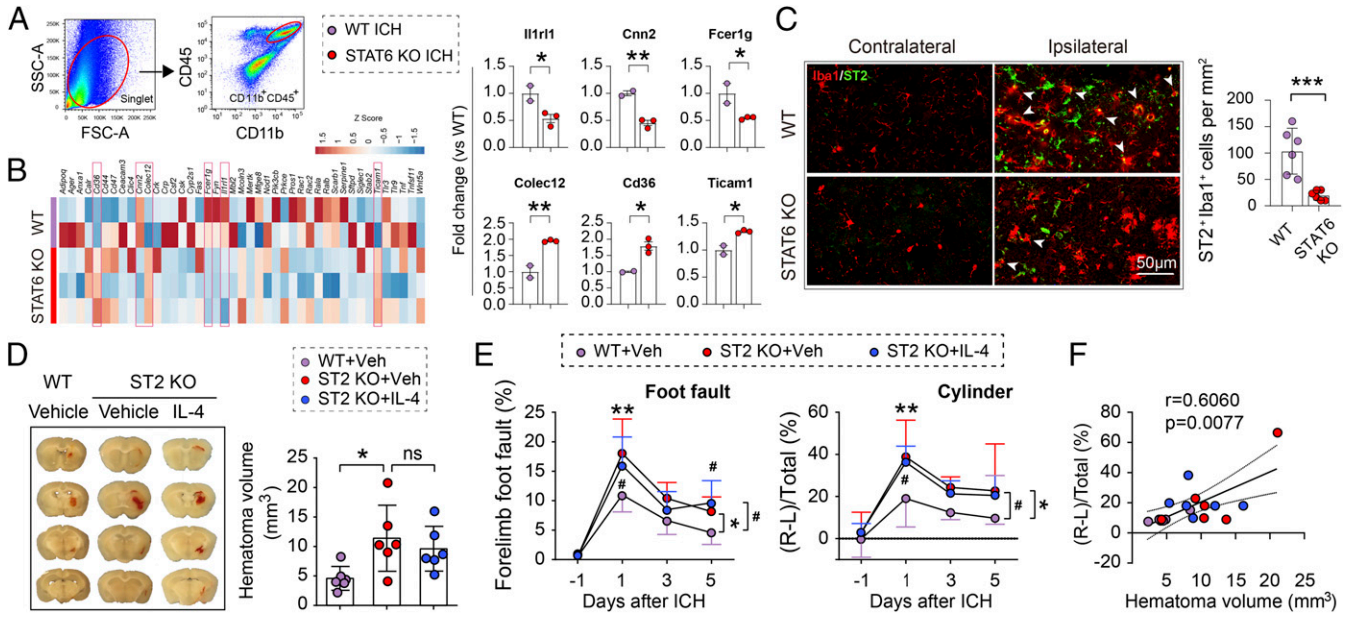

Fig. 8. ST2 as a signaling molecule downstream of STAT6 in facilitating hematoma resolution after ICH. ICH was induced in WT and STAT6 KO mice by blood injections into the right striatum. $CD45^{hi}CD11b^{+}$ microglia/macrophages were sorted from the ipsilateral brain 5 d after ICH. PCR arrays were used to analyze the differential expression of genes related to phagocytosis. (*A*) Representative plots illustrate the gating strategy for the FACS sorting of $CD45^{+}CD11b^{+}$ cells from ischemic brain. (*B*, *Left*) Heatmap showing PCR array expression profiles of 45 detected genes involved in phagocytosis regulation. $n = 2$ to 3 biological replicates per group, each sample pooled from 3 mice. (*Right*) Genes differentially expressed between STAT6 KO and WT mice after ICH ($P < 0.05$ by t test, indicated by red boxes in heatmap) are further presented in the form of mean ± SD (*C*, *Left*) Representative images of immunofluorescent staining of ST2 expression on $Iba1^{+}$ macrophages/activated microglia. (*Right*) Quantification of $Iba1^{+}ST2^{+}$ cells in the perihematoma regions 5 d after ICH. (*D*) ICH was induced in WT and ST2 KO mice by blood injection into the right striatum. IL-4 nanoparticles were applied intranasally starting 2 h after ICH and repeated daily for 4 d. (*Left*) Representative coronal brain sections show the intracerebral hematoma 5 d after ICH. (*Right*) Quantification of hematoma volumes on brain sections. $n = 6$ per group. Note that hematoma volumes were significantly larger in ST2 KO mice compared to WT mice, whereas IL-4 treatment failed to reduce hematoma volumes in ST2 KO mice. (*E*) Sensorimotor functions were assessed by foot fault (*Left*) and cylinder (*Right*) tests before ICH (−1 d) and 1, 3, and 5 d after ICH. $n = 6$ per group. (*F*) Spearman correlation analysis between the cylinder test and hematoma volumes 5 d after ICH. $^{*}P < 0.05$, $^{**}P < 0.01$, $^{***}P < 0.001$ ST2 KO vehicle vs. WT vehicle or as indicated, $\#P < 0.05$ ST2 KO+IL4 vs. WT vehicle by Student's t test (*B* and *C*), one-way ANOVA (*D*), or two-way repeated measures ANOVA (*E*) and Bonferroni post hoc tests. ns, not significant. The asterisks at the right indicate the group differences. The asterisks on the top indicate single day comparison between the two groups.

groups (WT, ST2 KO, ST2 KO + IL4 treatment) at 5 d after ICH ($r = 0.606$, $P = 0.0077$) (Fig. 8*F*).

Taken together, the results suggest that ST2 is a downstream molecule for STAT6 activation in microglia and macrophages, which mediates IL-4–afforded hematoma clearance and neurofunctional recovery after ICH.

Discussion

The present study identified a previously undefined role of STAT6 in promoting innate hematoma clearance and long-term neurological recovery in two independent murine models of ICH. Genetic ablation of STAT6 markedly impaired hematoma resolution and neurological performance, whereas intranasal delivery of IL-4 in WT mice resulted in augmentation of STAT6 activation in activated microglia and infiltrated macrophages and enhanced their capability for erythrocyte clearance and tissue protection after ICH. The expression of ST2, a recognized pro-phagocytotic molecule, was suppressed in STAT6 KO microglia/macrophages after ICH, and intranasal IL-4 treatment was ineffective when either STAT6 or ST2 signaling was absent. Collectively, these data support a prominent role for the IL-4/STAT6/ST2 signaling axis in improving the histological and neurofunctional outcomes after ICH.

It has been reported that the collagenase model and the blood-infusion model of ICH may result in similar hematoma volumes with dramatic histological differences (32). The rate of hematoma formation is rapid in the blood-injection model in contrast to a gradual evolution in the collagenase-injection model. In addition, the hematoma resolution in the blood-injection model is faster, which is accompanied by a quicker functional recovery compared to the collagenase-injection model. As the rapid hematoma formation in the blood-injection model better simulates the rapid blood accumulation after an abrupt blood vessel rupture in ICH patients, we mainly used this model in the present study. The key conclusions regarding the roles of STAT6 in hematoma resolution and functional recovery were confirmed in both models.

Endogenous hematoma clearance after ICH is mainly achieved by RBC lysis and phagocytosis of RBCs and RBC debris. Erythrolysis occurs as early as 24 h post-ICH (27). While the uncontrolled breakdown of RBCs might lead to the release of cytotoxic substances and a surge of oxidative stress, the rapid phagocytic clearance of RBCs by microglia and macrophages appears to temporally and spatially confine potentially harmful RBC-derived products and thus limit secondary brain damage (33). In our study, we observed correlations between hematoma size and hematoma clearance with neurological deficits in different cohorts of ICH animals with different genetic modifications (WT, STAT6 KO, or ST2 KO) with IL-4 (Figs. 1 *K–N* and 3*F*) or cell treatment (Fig. 7 *H* and *I*), strongly supporting the importance of hematoma resolution in the functional recovery after ICH.

The observed effects of STAT6 in innate hematoma resolution suggest a prophagocytic role for this protein. We found that STAT6 activation in microglia/macrophages commenced on day 3, peaked at day 5, and lasted for at least 7 d after ICH, a

temporal profile consistent with the time course of hematoma clearance. The demonstrated activation of STAT6 in microglia/macrophages but not in other CNS cells suggest a dominant role of STAT6 in brain phagocytes after ICH. Although a paucity of specific markers for microglia vs. macrophages hampers attempts to distinguish these two cell populations, a recent study using bone marrow chimeric mice showed that the loss of C-C chemokine receptor type 2 (Ccr2) in hematopoietic cells inhibited peripheral macrophage infiltration into the ICH brain (34). With fewer macrophages recruited to the brain, Ccr2 KO bone marrow chimeras suffered larger residual hematomas and worse functional recovery than WT chimeras after blood injections. Consistent with these findings, our data highlight the importance of STAT6 in infiltrated macrophages in erythrophagocytosis after ICH. Meanwhile, we found that residential microglia also play critical roles in hematoma resolution. In bone marrow chimera mice with WT CNS cells and GFP^+ bone marrows, both GFP^+Iba1^+ macrophages and GFP^-Iba1^+ microglia were detected in perihematoma regions. Furthermore, bone marrow chimera mice with STAT6 deficiency specifically in either CNS or peripheral immune cells significantly increased iron accumulation and worsened neurological deficits in the ICH brain. However, STAT6 expression is not restricted to microglia/macrophages. Rather, it is widely distributed among other immune cells, especially T cells. Therefore, neither global STAT6 KO mice nor bone marrow chimera mice can confirm that STAT6 functions exclusively in phagocytes. Nevertheless, both in vivo and in vitro phagocytosis assays revealed significant effects of STAT6 in RBC engulfment by macrophages and microglia.

Notably, in bone marrow chimera mice with WT CNS cells and GFP^+ bone marrows, the GFP^+Iba1^+ macrophages significantly outnumber the GFP^-Iba1^+ cells. It is known that some infiltrated macrophages in an injured brain do not express CX3CR1 (35). Therefore, it is possible that the GFP^-Iba1^+ cells in the brains of chimera mice include not only microglia but also GFP^- macrophages. This will further confirm the dominant number of macrophages in the ICH brain. The adoptive transfer of WT, but not STAT6-deficient macrophages, into STAT6 KO mice improved hematoma resolution and iron clearance, which supports the importance of STAT6-active macrophages in erythrophagocytosis after ICH. Furthermore, the adoptive transfer of WT macrophages rescued the poorer sensorimotor functions manifested by STAT6 KO mice, further supporting the role of STAT6-active macrophages in promoting functional recovery after ICH. The WT macrophage-afforded improvement in functional outcomes appears to be attributed to its hematoma resolution effect, as a significant correlation between hematoma clearance and sensorimotor performance was observed in macrophage-transferred STAT6 KO mice at 14 d after ICH (Fig. 7 *H* and *I*). However, such a correlation was not present at 5 d after ICH (Fig. 7*G*). It is therefore possible that both macrophages and microglia are needed to achieve the full capacity for hematoma clearance during the first 5 d following ICH. Alternatively, macrophage STAT6 may influence ICH outcomes through mechanisms in addition to erythrophagocytosis. For example, we found that STAT6 expression maintains macrophage/activated microglia in an antiinflammatory state in the ICH brain 5 d after ICH (Fig. 5*E*). We did not observe significant changes in the levels of proinflammatory factors in macrophage/activated microglia between STAT6 KO and WT mice 5 d after ICH. However, it is noted that IL-4, the best-known inducer for antiinflammatory phenotypes, was down-regulated in STAT6 KO macrophage/activated microglia after ICH (Fig. 5*E*). This may lead to a vicious cycle that further shifts STAT6 KO microglia/macrophages toward a detrimental phenotype that is associated with increased release of proinflammatory cytokines and reduced production of trophic factors for functional recovery in the late stage of ICH. In support of the function of STAT6 in neuroinflammation, a recent study documented that intracerebral injection of IL-4 promotes "alternative" activation of microglia/macrophages after ICH (36).

Transcriptional analysis of microglia/macrophages isolated from ICH brains revealed significant changes in an array of phagocytosis-related genes, including *Il1rl1*, *CD36*, and *Fcer1g*, in STAT6 KO mice vs. WT mice early after ICH, which reflect the importance of STAT6 in the signaling control of phagocytosis. We noted that *Il1rl1*, the gene that encodes the ST2 subunit of the IL-33 receptor, was significantly down-regulated in STAT6 KO phagocytes, suggesting a potential selective influence of STAT6 on ST2 expression in phagocytes of the ICH brain. Indeed, immunostaining confirmed that the expression of the ST2 protein was down-regulated in microglia/macrophages after ICH in STAT6 KO mice compared to WT mice. Recent studies demonstrated that IL-33/ST2 signaling promotes the phagocytotic activity of microglia under physiological and pathological conditions. For example, astrocyte-released IL-33 enhances microglia-mediated phagocytosis of synapses and maintains synapse homeostasis during CNS development (37). IL-33 also enhances microglial clearance of β-amyloid by activating the ST2/p38 signaling, reducing cerebral inflammation and rescuing memory deficits in Alzheimer's disease models (38). The data presented here provide direct evidence that ST2 is functionally important in hematoma clearance after ICH, as ST2 deficiency impaired hematoma resolution in brain parenchyma and worsened sensorimotor functions after ICH. Consistent with our findings, administration of the agonist of ST2 (IL-33) has been shown to provide neuroprotection in collagenase-induced ICH (39). IL-33 has also been reported to reduce neuronal damage and white matter injury through inhibiting microglial polarization in a rat blood model of ICH (39). In the present study, ST2 deficiency also significantly reduced the salutary effect of IL-4 on hematoma clearance, suggesting that ST2 is a key molecule downstream of STAT6 activation. How STAT6 impacts ST2 activity remains unknown, but several STAT6-binding elements [with a palindromic consensus sequence $TTC(N)_{3-4}GAA$] (30) are identified in the promoter region of ST2, indicating that ST2 may be a direct transcriptional target for STAT6. Further biochemical studies are warranted to fully understand the molecular interactions between STAT6, ST2, and other molecules in the context of ICH-induced activation of microglia and macrophages.

In addition to microglia/macrophages, the IL-4/STAT6 signaling may target other immune cells to indirectly enhance hematoma resolution. For example, the blood or thymus T cells are known to shift microglia and macrophages polarization in CNS diseases (40, 41). The IL-4/STAT6 axis has been suggested to regulate T cell-mediated immune responses in blood, thymus, and other peripheral lymph organs (42–44), and may therefore adjust microglia/macrophage phenotype. Future studies are warranted to explore the involvement of other immune cells in IL-4/STAT6-afforded neuroprotection after ICH. The multitargeting capacities of IL-4/STAT6 will make it an excellent therapy for CNS injuries.

Despite many endeavors to elucidate the mechanisms underlying ICH-induced brain injury and to identify therapeutic targets for ICH, no drug therapy is currently available for this devastating medical condition. Recently, a multicenter, double-blind, randomized, placebo-controlled futility trial (iDEF) examined the effect of deferoxamine in ICH patients, based on numerous preclinical studies showing protective effects of iron chelators on neurobehavioral performance and mortality after ICH (45–47). The phase 2 iDEF trial found that intermediate doses of deferoxamine, although safe and well tolerated in ICH patients, did not have sufficient effect on ICH 90-d outcomes to justify proceeding to a definitive, phase 3 clinical trial (48). We report here that IL-4 treatment after ICH augments RBC clearance and limits iron deposition through, or at least

associated with a significant increase in STAT6 activation status. It will be interesting to test the effect of combined treatments of IL-4 with deferoxamine, the MISTIE procedure, or other forms of mechanical hematoma removal in our future study. Such combined treatment may achieve additive or even synergistic therapeutic effects by decreasing the source of iron and simultaneously enhancing its removal/detoxification. In addition to its actions on microglia/macrophages, IL-4 may also target other immune cells that are known to impact ICH outcomes, such as infiltrated T cells and neutrophils (49). Moreover, boosting antiinflammatory responses in the lesioned brain through STAT6 activation will promote brain repair and recovery.

The nasal delivery of lipid nanoparticles has been increasingly applied for CNS drugs because it allows direct nose-to-brain delivery and avoids gastrointestinal and hepatic first-pass metabolism (50). We recently showed that intranasally delivered IL-4 nanoparticles can reach the brain cortex and subcortical white matter (26). The nasal route may serve as a noninvasive pragmatic form of therapeutic intervention for a critically ill ICH patient population, which may increase IL-4 brain penetration, reduce systemic bystander effects, and facilitate its clinical translation. Given these collective observations, intranasal IL-4 is worthy of continued investigation as a potential new therapy for ICH.

Materials and Methods

Key resources that are essential to reproduce the results are in *SI Appendix*, Table S1. ICH was induced in adult male or female mice (10- to 12-wk old, 25 to 30 g) or aged male (18-mo old) mice. All animal procedures were approved by the University of Pittsburgh Institutional Animal Care and Use Committee and performed in accordance with the *Guide for the Care and Use of Laboratory Animals* (51). All efforts were made to minimize animal suffering and the number of animals used. Surgeries and all outcome assessments were performed by investigators blinded to mouse genotype and experimental group assignments. All statistics are summarized in *SI Appendix*, Table S2.

For further methodological details, please consult *SI Appendix*.

Data Availability. All study data are included in the article and supporting information.

ACKNOWLEDGMENTS. We thank T. Kevin Hitchens and Lesley M. Foley for assistance with the MRI experiments and Patricia Strickler for administrative support. The ST2 knockout breeders were a gift from A. McKenzie (Medical Research Council as part of UK Research and Innovation). This project was supported by the University of Pittsburgh School of Medicine. J.C. is the Richard King Mellon Professor of Neurology and a recipient of a VA Senior Research Career Scientist Award. M.V.L.B. is the Sylvia and Robert S. Olnick Professor of Neuroscience.

1. R. V. Krishnamurthi *et al.*; Global Burden of Diseases, Injuries, Risk Factors Study 2010 (GBD 2010); GBD Stroke Experts Group, Global and regional burden of first-ever ischaemic and haemorrhagic stroke during 1990-2010: Findings from the Global Burden of Disease Study 2010. *Lancet Glob. Health* **1**, e259-81 (2013).
2. D. A. Cadilhac, H. M. Dewey, T. Vos, R. Carter, A. G. Thrift, The health loss from ischemic stroke and intracerebral hemorrhage: Evidence from the North East Melbourne Stroke Incidence Study (NEMESIS). *Health Qual. Life Outcomes* **8**, 49 (2010).
3. V. Hachinski *et al.*, Stroke: Working toward a prioritized world agenda. *Stroke* **5**, 238–256 (2010).
4. J. Broderick *et al.*; American Heart Association; American Stroke Association Stroke Council; High Blood Pressure Research Council; Quality of Care and Outcomes in Research Interdisciplinary Working Group, Guidelines for the management of spontaneous intracerebral hemorrhage in adults: 2007 update: A guideline from the American Heart Association/American Stroke Association Stroke Council, High Blood Pressure Research Council, and the Quality of Care and Outcomes in Research Interdisciplinary Working Group. *Stroke* **38**, 2001–2023 (2007).
5. V. L. Feigin *et al.*; GBD 2013 Writing Group; GBD 2013 Stroke Panel Experts Group, Update on the global burden of ischemic and hemorrhagic stroke in 1990-2013: The GBD 2013 study. *Neuroepidemiology* **45**, 161–176 (2015).
6. R. V. Krishnamurthi *et al.*; Global Burden of Diseases, Injuries, and Risk Factors 2010 Study Stroke Expert Group, The global burden of hemorrhagic stroke: A summary of findings from the GBD 2010 study. *Glob. Heart* **9**, 101–106 (2014).
7. C. J. van Asch *et al.*, Incidence, case fatality, and functional outcome of intracerebral haemorrhage over time, according to age, sex, and ethnic origin: A systematic review and meta-analysis. *Lancet Neurol.* **9**, 167–176 (2010).
8. M. T. Poon, A. F. Fonville, R. Al-Shahi Salman, Long-term prognosis after intracerebral haemorrhage: Systematic review and meta-analysis. *J. Neurol. Neurosurg. Psychiatry* **85**, 660–667 (2014).
9. J. C. Hemphill 3rd *et al.*; American Heart Association Stroke Council; Council on Cardiovascular and Stroke Nursing; Council on Clinical Cardiology, Guidelines for the management of spontaneous intracerebral hemorrhage: A guideline for healthcare professionals from the American Heart Association/American Stroke Association. *Stroke* **46**, 2032–2060 (2015).
10. D. F. Hanley *et al.*; MISTIE III Investigators, Efficacy and safety of minimally invasive surgery with thrombolysis in intracerebral haemorrhage evacuation (MISTIE III): A randomised, controlled, open-label, blinded endpoint phase 3 trial. *Lancet* **393**, 1021–1032 (2019).
11. J. P. Broderick, T. G. Brott, J. E. Duldner, T. Tomsick, G. Huster, Volume of intracerebral hemorrhage. A powerful and easy-to-use predictor of 30-day mortality. *Stroke* **24**, 987–993 (1993).
12. A. D. Mendelow *et al.*; STICH II Investigators, Early surgery versus initial conservative treatment in patients with spontaneous supratentorial lobar intracerebral haematomas (STICH II): A randomised trial. *Lancet* **382**, 397–408 (2013).
13. A. D. Mendelow *et al.*; STICH investigators, Early surgery versus initial conservative treatment in patients with spontaneous supratentorial intracerebral haematomas in the international Surgical Trial in Intracerebral Haemorrhage (STICH): A randomised trial. *Lancet* **365**, 387–397 (2005).
14. P. Vespa *et al.*; ICES Investigators, ICES (intraoperative stereotactic computed tomography-guided endoscopic surgery) for brain hemorrhage: A multicenter randomized controlled trial. *Stroke* **47**, 2749–2755 (2016).
15. N. Chaudhary, A. S. Pandey, X. Wang, G. Xi, Hemorrhagic stroke—Pathomechanisms of injury and therapeutic options. *CNS Neurosci. Ther.* **25**, 1073–1074 (2019).
16. T. Garton, R. F. Keep, Y. Hua, G. Xi, Brain iron overload following intracranial haemorrhage. *Stroke Vasc. Neurol.* **1**, 172–184 (2016).
17. A. L. A. Garton, V. P. Gupta, B. R. Christophe, E. S. Connolly, Jr, Biomarkers of functional outcome in intracerebral hemorrhage: Interplay between clinical metrics, CD163, and ferritin. *J. Stroke Cerebrovasc. Dis.* **26**, 1712–1720 (2017).
18. J. Wang, S. Doré, Heme oxygenase-1 exacerbates early brain injury after intracerebral haemorrhage. *Brain* **130**, 1643–1652 (2007).
19. M. Xue, M. R. Del Bigio, Intracerebral injection of autologous whole blood in rats: Time course of inflammation and cell death. *Neurosci. Lett.* **283**, 230–232 (2000).
20. R. A. Taylor *et al.*, TGF-β1 modulates microglial phenotype and promotes recovery after intracerebral hemorrhage. *J. Clin. Invest.* **127**, 280–292 (2017).
21. R. M. Dahnovici *et al.*, Microscopic aspects of macrophage system cells in hemorrhagic stroke in humans. *Rom. J. Morphol. Embryol.* **52**, 1249–1253 (2011).
22. X. Zhao, J. Grotta, N. Gonzales, J. Aronowski, Hematoma resolution as a therapeutic target: The role of microglia/macrophages. *Stroke* **40** (suppl.(3), S92–S94 (2009).
23. X. Zhao *et al.*, Hematoma resolution as a target for intracerebral hemorrhage treatment: Role for peroxisome proliferator-activated receptor gamma in microglia/macrophages. *Ann. Neurol.* **61**, 352–362 (2007).
24. K. Vaibhav *et al.*, Remote ischemic post-conditioning promotes hematoma resolution via AMPK-dependent immune regulation. *J. Exp. Med.* **215**, 2636–2654 (2018).
25. X. Zhao *et al.*, Cleaning up after ICH: The role of Nrf2 in modulating microglia function and hematoma clearance. *J. Neurochem.* **133**, 144–152 (2015).
26. Q. Zhang *et al.*, The interleukin-4/PPARγ signaling axis promotes oligodendrocyte differentiation and remyelination after brain injury. *PLoS Biol.* **17**, e3000330 (2019).
27. G. Dang *et al.*, Early erythrolysis in the hematoma after experimental intracerebral hemorrhage. *Transl. Stroke Res.* **8**, 174–182 (2017).
28. G. B. Chavhan, P. S. Babyn, B. Thomas, M. M. Shroff, E. M. Haacke, Principles, techniques, and applications of T2*-based MR imaging and its special applications. *Radiographics* **29**, 1433–1449 (2009).
29. N. Chaudhary *et al.*, Brain tissue iron quantification by MRI in intracerebral hemorrhage: Current translational evidence and pitfalls. *J. Cereb. Blood Flow Metab.* **39**, 562–564 (2019).
30. S. Goenka, M. H. Kaplan, Transcriptional regulation by STAT6. *Immunol. Res.* **50**, 87–96 (2011).
31. J. M. Buckley *et al.*, Increased susceptibility of ST2-deficient mice to polymicrobial sepsis is associated with an impaired bactericidal function. *J. Immunol.* **187**, 4293–4299 (2011).
32. C. L. MacLellan *et al.*, Intracerebral hemorrhage models in rat: Comparing collagenase to blood infusion. *J. Cereb. Blood Flow Metab.* **28**, 516–525 (2008).
33. A. R. Saand, F. Yu, J. Chen, S. H. Chou, Systemic inflammation in hemorrhagic strokes—A novel neurological sign and therapeutic target? *J. Cereb. Blood Flow Metab.* **39**, 959–988 (2019).
34. C. F. Chang *et al.*, Erythrocyte efferocytosis modulates macrophages towards recovery after intracerebral hemorrhage. *J. Clin. Invest.* **128**, 607–624 (2018).
35. L. Garcia-Bonilla *et al.*, Spatio-temporal profile, phenotypic diversity, and fate of recruited monocytes into the post-ischemic brain. *J. Neuroinflammation* **13**, 285 (2016).
36. J. Yang *et al.*, Interleukin-4 ameliorates the functional recovery of intracerebral hemorrhage through the alternative activation of microglia/macrophage. *Front. Neurosci.* **10**, 61 (2016).
37. I. D. Vainchtein *et al.*, Astrocyte-derived interleukin-33 promotes microglial synapse engulfment and neural circuit development. *Science* **359**, 1269–1273 (2018).
38. A. K. Fu *et al.*, IL-33 ameliorates Alzheimer's disease-like pathology and cognitive decline. *Proc. Natl. Acad. Sci. U.S.A.* **113**, E2705–E2713 (2016).

39. Y. Gao *et al*., IL-33 exerts neuroprotective effect in mice intracerebral hemorrhage model through suppressing inflammation/apoptotic/autophagic pathway. *Mol. Neurobiol.* **54**, 3879–3892 (2017).
40. R. K. Sheean *et al*., Effect of thymic stimulation of CD4+ T cell expansion on disease onset and progression in mutant SOD1 mice. *J. Neuroinflammation* **12**, 40 (2015).
41. K. Mittal *et al*., CD4 T cells induce A subset of MHCII-expressing microglia that attenuates Alzheimer pathology. *iScience* **16**, 298–311 (2019).
42. J. T. Walsh *et al*., MHCII-independent CD4+ T cells protect injured CNS neurons via IL-4. *J. Clin. Invest.* **125**, 2547 (2015).
43. E. Maier *et al*., Inhibition of suppressive T cell factor 1 (TCF-1) isoforms in naive CD4+ T cells is mediated by IL-4/STAT6 signaling. *J. Biol. Chem.* **286**, 919–928 (2011).
44. H. Shen *et al*., Recirculating Th2 cells induce severe thymic dysfunction via IL-4/STAT6 signaling pathway. *Biochem. Biophys. Res. Commun.* **501**, 320–327 (2018).
45. Q. Li *et al*., Neuroprotection of brain-permeable iron chelator VK-28 against intracerebral hemorrhage in mice. *J. Cereb. Blood Flow Metab.* **37**, 3110–3123 (2017).
46. W. Ni *et al*., Deferoxamine reduces intracerebral hemorrhage-induced white matter damage in aged rats. *Exp. Neurol.* **272**, 128–134 (2015).
47. X. Duan, Z. Wen, H. Shen, M. Shen, G. Chen, Intracerebral hemorrhage, oxidative stress, and antioxidant therapy. *Oxid. Med. Cell. Longev.* **2016**, 1203285 (2016).
48. M. Selim *et al*.; i-DEF Investigators, Deferoxamine mesylate in patients with intracerebral haemorrhage (i-DEF): A multicentre, randomised, placebo-controlled, double-blind phase 2 trial. *Lancet Neurol.* **18**, 428–438 (2019).
49. X. Zhao *et al*., Neutrophil polarization by IL-27 as a therapeutic target for intracerebral hemorrhage. *Nat. Commun.* **8**, 602 (2017).
50. S. Cunha, M. H. Amaral, J. M. S. Lobo, A. C. Silva, Lipid nanoparticles for nasal/intranasal drug delivery. *Crit. Rev. Ther. Drug Carrier Syst.* **34**, 257–282 (2017).
51. National Research Council, *Guide for the Care and Use of Laboratory Animals* (National Academies Press, Washington, DC, ed. 8, 2011).